Journal of Power Sources 187 (2009) 620–626

Contents lists available at ScienceDirect

Journal of Power Sources

journal homepage: www.elsevier.com/locate/jpowsour

Triphenylamine-based organic dye containing the diphenylvinyl and rhodanine-3-acetic acid moieties for efficient dye-sensitized solar cells

Juan Pei, Shengjie Peng, Jifu Shi, Yanliang Liang, Zhanliang Tao, Jing Liang, Jun Chen*

Institute of New Energy Material Chemistry and Key Laboratory of Energy-Material Chemistry, Chemistry College, Nankai University, Tianjin 300071, People's Republic of China

ARTICLE INFO

Article history:
Received 21 September 2008
Received in revised form 25 October 2008
Accepted 5 November 2008
Available online 18 November 2008

Keywords:
Dye-sensitized solar cells
Triphenylamine-based dye
Electron transfer
Light-to-electricity conversion efficiency
Long-term stability

ABSTRACT

In this paper, we report on the synthesis, characterization of a new triphenylamine (TPA) derivative (TPAR14) with a "secondary electron transferring" structure as well as its application to dye-sensitized solar cells (DSCs). The introduction of diphenylvinyl to the adjacent phenyl ring of the TPA core could not only increase the extinction coefficient and λ_{max} by the extension of π-conjugation, but also form three-dimensional obstacle for dye aggregation and triiodide that is in favor of higher open-circuit photovoltage (V_{oc}). An overall light-to-electricity conversion efficiency of 6.27% is obtained for the DSC with the as-synthesized dye under AM 1.5 irradiation (100 mW cm^{-2}), which is the highest value among the TPA-rhodanine-3-acetic acid-based DSCs. The long-term stability test of TPAR14 under heat shows its character of high stability. The present work indicates that the as-synthesized TPAR14 is promising in the application of DSCs.

1. Introduction

Dye-sensitized solar cells (DSCs), which are one of the promising photovoltaic devices, have attracted a great interest since the precursory research in 1991 [1] for their potential low cost and relatively high light-to-electricity conversion efficiency (η). The heart of a DSC system is a mesoporous oxide layer composed of nanometer-sized particles anchored by a monolayer of the charge transfer dye [2,3]. The photosensitizers play a crucial role for the DSCs getting higher η and have been actively studied by researchers all over the world. Until now, the record efficiency of DSCs is kept by a polypyridyl ruthenium sensitizer (11%) in combination with a voltaic iodide/triiodide mixture as electrolyte [4]. In recent years, metal-free organic sensitizers have been developed by a few groups due to their advantages such as diversity of molecule structures, high molar extinction coefficient, simple synthesis as well as low cost and environmental issues [5–11].

Most of the organic sensitizers applied in DSCs show the character with both the electron donor (D) and the electron acceptor (A) linked by a π-conjugation bridge, which is called the D–π–A structure [12]. Generally, organic dyes for excellent DSCs are required to possess broad and intense spectral absorption in the visible light region and have suited excited-state redox potential with the energy of the conduction band edge. The major factors for low conversion efficiency of DSCs based on organic dyes are the formation of dye aggregation on the semiconductor surface and the recombination of conduction band electrons with triiodide in the electrolyte [13].

Recently, a nonplanar triphenylamine (TPA) moiety with famous electron-donating nature [14] as electron donor into the organic framework was proposed [15–17]. In the meantime, rhodanine-3-acetic acid moiety is used as a common electron acceptor/anchoring group in organic sensitizers, and the highest conversion efficiency of 9.03% was attained for the DSC with indole-based organic dyes [18]. However, DSCs based on dyes with TPA donor and rhodanine-3-acetic acid acceptor have only reached the efficiencies in the range of 1.27–5.84%. As we know, introducing a secondary electron transfer function is a possible alternative to retard the interfacial charge-recombination dynamics and to retain efficient light-induced charge separation [19,20]. Thus, it is interesting to study a further influence by introducing a secondary electron transfer function to the sensitizer with TPA as the electron donor and rhodanine-3-acetic acid moiety as the electron acceptor.

In this paper, we have designed and synthesized a new TPA derivative (TPAR14), as shown in Fig. 1. The character of this dye is in the combination of an introduction of diphenylvinyl to the adjacent phenyl ring of the TPA core and the rhodanine-3-acetic acid moiety as the acceptor. The as-synthesized dye shows the photovoltaic performances with a short-circuit photocurrent density (J_{sc}) of 15.5 mA cm^{-2}, an open-circuit voltage (V_{oc}) of 0.64 V, and a fill factor (FF) of 0.63, corresponding to the light-to-electricity conversion efficiency of 6.27% under AM 1.5 irradiation with 100 mW cm^{-2} simulated sunlight. This is the highest value among the TPA-rhodanine-3-acetic acid-based DSCs till now. The present results

* Corresponding author. Tel.: +86 22 23506808; fax: +86 22 23506808.
E-mail address: chenabc@nankai.edu.cn (J. Chen).

0378-7753/$ – see front matter © 2008 Elsevier B.V. All rights reserved.
doi:10.1016/j.jpowsour.2008.11.028

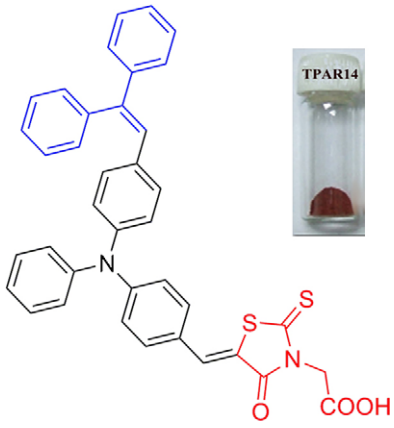

Fig. 1. Molecular structure of the triphenylamine-based dye (TPAR14). The substituted electron donating and withdrawing groups have been marked by colour drawing. Insert image is the powder photograph of the as-synthesized dye (in glass bottle). (For interpretation of the references to colour in this figure legend, the reader is referred to the web version of the article.)

indicate that this metal-free organic dye of TPAR14 is promising in the development of DSCs.

2. Experimental

2.1. Materials and reagents

THF was distilled from sodium/benzophenone. DMF and $POCl_3$ were distilled from CaH_2 under N_2 atmosphere. Potassium *tert*-butoxide (*t*-BuOK), rhodanine-3-acetic acid and 4-*tert*-butylpyridine (TBP) were purchased commercially with analytical grade. Tetrabutylammonium perchlorate (TBAP) and 1,2-dimethyl-3-propylimidazolium iodide (DMPImI) were synthesized and purified according to literature [21,22]. All other solvents and chemicals used in this work were analytical grade and used without further purification. The substrates of transparent conducting oxide glass (TCO, F-doped SnO_2, 20 Ω sq^{-1}, Yaohua company of China) were washed with basic solution, diluted nitric acid, ethanol, and acetone successively under supersonication for 30 min each before use. Commercial TiO_2 (P25, a mixture of 30% rutile and 70% anatase, Degussa AG, Germany) was used for the preparation of the nanocrystalline films. All chromatographic separations were carried out on silica gel (200–300 mesh).

2.2. Dye synthesis

The dye based on diphenylvinyl triphenylamine (TPAR14) was synthesized by Knoevenagel condensation reaction [23] of the 4-(*N*-phenyl-*N*-(4-(2,2-diphenylvinyl)phenyl)amino)benzaldehyde (**1**) and rhodanine-3-acetic acid. The intermediate (**1**) was prepared from 4,4′-(phenylazanediyl)dibenzaldehyde and (diphenylmethyl)triphenylphosphonium bromide by Wittig reaction [24]. The starting material 4,4′-(phenylazanediyl)dibenzaldehyde was prepared by treating TPA with $POCl_3$ in DMF according to literature procedure [25].

2.2.1. 4-(N-phenyl-N-(4-(2,2-diphenylvinyl)phenyl)amino)benzaldehyde (*1*)

To a 50 ml THF solution including 3 g of (diphenylmethyl)triphenylphosphonium bromide and 1.2 g of 4,4′-(phenylazanediyl)dibenzaldehyde, 0.66 g *t*-BuOK was added at room temperature. The red solution was allowed to stand for 24 h under refluxing. After filtered, the THF solution was evaporated using rotary evaporator and the pure product **1** was obtained by silica gel chromatography (eluent petroleum ether: ethyl acetate = 9:1, R_f = 0.3) to afford 0.81 g of yellow dope in 45% yield. IR (KBr): 3431, 1723, 1690, 1587, and 1025. ^{1}H NMR (300 MHz, DMSO-d_6): δ (ppm) 9.77 (s, 1H), 7.72 (d, J = 9.0 Hz, 2H), 7.32–7.44 (m, 8H), 7.19–7.29 (m, 4H), 7.16 (d, J = 7.2 Hz, 2H), 7.12 (s, 1H), 7.09 (s, 1H), 7.01 (d, J = 8.8 Hz, 2H), 6.85–6.92 (m, 4H). ^{13}C NMR (150 MHz, $CDCl_3$): 190.44, 153.07, 145.00, 144.64, 143.86, 142.26, 140.40, 133.91, 131.27, 130.73, 130.21, 129.75, 128.83, 128.51, 128.26, 127.58, 126.57, 125.04, and 119.95. EIS-MS: m/z $[M+H]^+$ 452. Anal. Calcd. for $C_{33}H_{25}ON$: C 87.8%, N 3.1%, H 5.58%; found: C 88.1%, N 3.4%, H 5.4%.

2.2.2. 2-(5-(4-(N-Phenyl-N-(4-(2,2′-diphenylvinyl)phenyl)amino)benzylidene)-4-oxo-2-thioxothiazolidin-3-yl)acetic acid (TPAR14)

1 (248 mg, 0.55 mmol) and rhodanine-3-acetic acid (110 mg, 0.57 mmol) were added into 15 ml glacial acetic acid and refluxed for 4 h in the presence of 100 mg ammonium acetate. After cooling to room temperature, the mixture was poured into ice water. The precipitate was filtered and washed with distilled water. After drying under vacuum, the resulting precipitate was dissolved in ethyl acetate solution. By dropping petroleum ether in, the red crystals of TPAR14 were obtained (240 mg, 70%), mp 219.7 °C. IR (KBr): 3438, 2924, 2850, 1713, 1634, 1576, 1503, and 1295. ^{1}H NMR (300 MHz, DMSO-d_6): δ (ppm) 7.76 (s, 1H), 7.54 (d, J = 9.0, 2H), 7.38–7.47 (m, 5H), 7.29–7.35 (m, 5H), 7.13–7.25 (m, 5H), 7.09 (s, 1H), 7.01 (d, J = 8.7, 2H), 6.89–6.92 (m, 4H), 4.72 (s, 2H). ^{13}C NMR (75 MHz, DMSO-d_6): 193.55, 168.00, 167.14, 150.45, 145.90, 144.80, 143.05, 141.88, 140.61, 134.13, 133.55, 131.38, 130.76, 130.24, 129.84, 129.07, 128.41, 127.58, 127.06, 126.28, 125.50, 120.45, 118.02, and 45.60. ESI-MS: m/z $[M-H]^-$ 623. Anal. Calcd. for $C_{38}H_{28}N_2O_3S_2$: C 72.75%, N 4.38%, H 4.4%; found: C 73.0%, N 4.5%, H 4.5%.

2.3. Analytical measurements

^{1}H (300 MHz) and ^{13}C NMR (300 or 600 MHz) spectra were carried out with a Varian Mercury Vx300 spectrometer or Bruker Ultrashield 600 with the chemical shifts against tetramethylsilane (TMS). Electrospray ionization mass spectrometry (ESI-MS) spectra were measured with a LCQ AD (Thermofinnigan, USA) mass spectrometer. Elemental analysis was carried out on a Perkin-Elmer 2400 CHNS analyzer. The melting point was taken on a RY-1 thermometer. FT-IR spectrum of the new substances in the region of 4000–400 cm^{-1} were recorded on a Bio-Rad FTS 135 FT-IR spectrometer using KBr discs; while the IR spectrum of dye-loaded TiO_2 film was tested using the way of 30° reflection. The absorption spectra of the dye in methanol solution and absorbed on TiO_2 film were measured with a Jasco V-550 UV/vis spectrophotometer. The steady-state fluorescence spectrum of the dye in methanol solution was observed on a Cary Eclipse fluorescence spectrophotometer at ambient temperature. Thermogravimetric (TG) analysis of the dye was performed with a NETZSCH-TG 209 analyzer. The amount of the dye adsorbed on the TiO_2 surface was estimated spectroscopically after the dye had been desorbed in a 0.1 M solution of NaOH in methanol. The oxidation potential of the dye in acetonitrile was measured in a three-electrode system with a glassy carbon working electrode, a Pt-wire counter electrode, and a Ag/Ag^+ reference electrode which was calibrated with ferrocene [26]. The differential pulse voltammetry (DPV) measurements were performed with a PARSTAT 2273 electrochemical analyzer. The supporting electrolyte was 0.1 M TBAP in dry acetonitrile, which was purged with argon (99.999%) and stirred for 15 min prior to the scan.

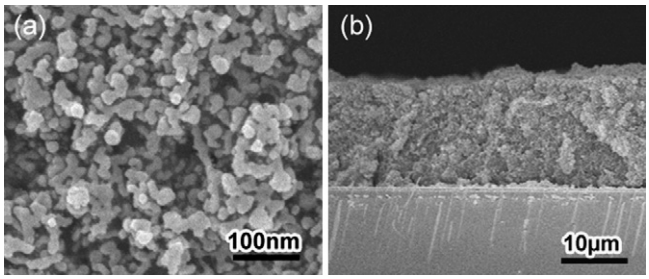

Fig. 2. SEM images of the surface (a) and the cross-section of the as-prepared nanostructured TiO_2 film coated on the conducting glass.

2.4. Computation methods

The geometrical and electronic properties of the TPAR14 were performed with the Gaussian 03 program package [27]. The calculation was optimized by means of the B3LYP method (Becke three parameters hybrid functional with Lee–Yang–Perdew correlation functionals) in combination with the Pople 6-31+G(d) atomic basis set. The excitation transitions of TPAR14 was calculated using time-dependent density functional theory (TD-DFT) calculations with B3LYP/6-31+G(d). Molecular orbitals were visualized using Gaussview.

2.5. Fabrication of the dye-sensitized TiO_2 electrodes

The washed FTO substrates were immersed into 50 mM $TiCl_4$ aqueous solution at 70 °C for 30 min to form a compact layer of TiO_2 with the thickness of about 100 nm, which plays an important role in suppressing the charge recombination of DSCs at the interface between FTO and electrolyte. Then, a thin film of TiO_2 was prepared on the FTO substrate with the compact TiO_2 layer through a screen-printing technique. The screen with a 420 mesh was made of polyester and the squeeze was plastic. The printed TiO_2 thin film was dried at ambient atmosphere for 5 min, followed by an annealing at 450 °C for half an hour. When the temperature was reduced to 30 °C, the film was taken out. The TiO_2 thin film with more layers was achieved by repeating the above screen-printing process. The surface of the as-prepared TiO_2 film is of porous character with nanoparticles (Fig. 2a), which benefits the adsorption of dyes. The cross-section analysis in Fig. 2b illustrates that the thickness of TiO_2 film is about 15 μm.

The as-prepared dye was dissolved at a concentration of 0.5 mM in a mixed solvent of 20:80 (vol%) acetonitrile and methanol. For comparison, 0.5 mM N3 dye in ethanol solution also prepared. The TiO_2 films were immersed in the dye-solutions when they were at ~70 °C cooled from the heating and kept at 25 °C for more than 12 h to allow the dyes to adsorb onto the TiO_2 surface.

2.6. Assembly of the cells and photovoltaic characterization

The electrochemical cell (two-electrode system) used for photovoltaic measurements consisted of a dye-sensitized TiO_2 electrode, a counter electrode, and an electrolyte. The electrolyte of 0.1 M LiI, 0.05 M I_2, 0.6 M DMPImI in acetonitrile was used for TPA dye TPAR14. However, for N3 dye 0.5 M TBP was added in. We used two types of cells, type A and B (Fig. 3). For the former, the two electrodes were spaced by adhesive tape (45 μm thick) with two black binder clips. The latter is a sealed cell with the two electrodes assembled into a sealed sandwich-type cell by heating with a hot-melt ionomer film (Syrlyn 1702, 60 μm thick) as a spacer between the electrodes. Then the holes drilled previously were sealed by using glass cement and a cover glass (1 mm thick) at room temperature.

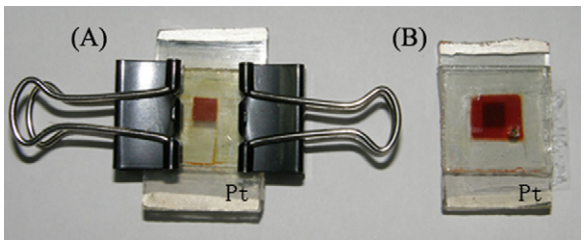

Fig. 3. Photograph of DSCs with type (A) and (B). Active area of the device was 0.16 cm^2.

Photoelectrochemical performance of the solar cell was measured using a Keithley 2400 digital source meter controlled by a computer [28]. A 500-W Xe lamp served as the light source in combination with a band-pass filter (400–800 nm) to remove ultraviolet and infrared radiation for giving 100 mW cm^{-2} at the surface of the test cell. The incident light intensity was calibrated by a radiometer. Further calibration was carried out by using a USB4000 plug-and-play miniature fiber optic spectrometer (Ocean Optics Inc., USA) to reduce the mismatch between the simulated and the true solar spectrum. The light-to-electricity conversion efficiency (η), which expresses the ratio of the produced maximum power (P_{max}) to the incoming power (P_{in}, mW cm^{-2}), can be measured by the following equation [19]:

$$\eta = \frac{P_{max}}{P_{in}} = \frac{J_{sc} V_{oc} FF}{P_{in}} \quad (1)$$

where J_{sc} is the short-circuit photocurrent density, V_{oc} is the open-circuit photovoltage, and FF is the fill factor of the cell. The incident-photon-to-electron conversion efficiency (IPCE) can be defined as the ratio of the produced electrons getting across the external circuit ($n_{electrons}$) to the injecting photons ($n_{photons}$). The IPCE values were measured under monochromatic light with 10 nm intervals according to the following equation [19]:

$$IPCE(\lambda) = \frac{n_{electrons}(\lambda)}{n_{photons}(\lambda)} = \frac{1240 I(\lambda)}{\lambda \phi(\lambda)} \quad (2)$$

where $I(\lambda)$ is the current given by the cell at wavelength λ and $\phi(\lambda)$ the incoming power at wavelength λ. The light from a 500-W Xe lamp was focused through a WDS-5 monochromator (TuoPu Instrument Co., Ltd., TianJin) onto the photovoltaic cell under testing. The IPCE values were determined between 400 and 800 nm.

3. Results and discussion

3.1. Photophysical properties

Fig. 4 shows the absorption spectrum of TPAR14 in methanol solution. From Fig. 4, it can be seen that the dye exhibits two distinct bands: one relatively weak band in the near-UV region (348 nm) corresponding to the π–π^* electron transition, and the other strong absorption in the visible region (468 nm) that can be assigned to an intramolecular charge transfer (ICT) between the TPA donating unit and the rhodanine-3-acetic acid anchoring moiety [29]. Noticeably, the molar extinction coefficient (4.47×10^4 M^{-1} cm^{-1}) is higher than that of N3 dye (1.42×10^4 M^{-1} cm^{-1} at 532 nm in ethanol) [30], indicating a good ability of light harvesting. When the TPAR14 dye is excited within its π–π^* band in an air-equilibrated methanol solution at 298 K, it exhibits strong luminescence maximum at 572 nm.

Fig. 5 shows the normalized absorbance of TPAR14 in methanol solution and adsorbed on TiO_2 film. In comparison to the spectrum in methanol solution, the absorption spectrum on TiO_2 film was broadened and red-shifted from 468 to 476 nm, indicating that the TPAR14 molecules were assembled on the TiO_2 film in

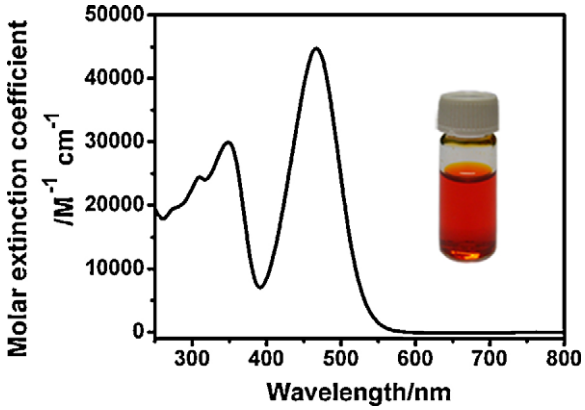

Fig. 4. UV–vis absorption spectrum of the dye measured in methanol solution with the concentration of 0.05 mM. The insert photograph shows the methanol solution in glass bottle.

a monolayer state with very little partial aggregation due to its three-dimensional structure. Therefore, it is needless to incorporate coadsorbents such as chenodeoxycholic acid (CDCA) to prevent dyes from aggregating on TiO_2 film. The amount of TPAR14 adsorbed on TiO_2 film is determined to be 2.0×10^{-7} M cm^{-2} by desorbing the dye with a basic solution. Based on both the normalized absorption and emission spectra in Fig. 5, the intersection wavelength λ_{0-0} of 511 nm is estimated to be 2.43 eV, which corresponds to E_{0-0} transition energy (zero–zero excited energy) value.

3.2. Mode of TPAR14 adsorbed on TiO_2 surface

The binding mode of dye molecules to the TiO_2 surface, which is associated with the interfacial electron injection, was analyzed by the FT-IR technique. Fig. 6 shows the FT-IR spectra for TPAR14 powder and TiO_2 film exposed to TPAR14 solution. For the dye powder, the 1713 and 1632 cm^{-1} peaks are attributed to the stretch band of the carboxyl group ν(COOH) and the carbonyl group in the rhodanine ring ν(C=O), respectively. In the case of rhodanine-3-acetic acid, a raw material of the dye, both the absorption peaks of ν(COOH) and ν(C=O) were observed at almost the same position at 1750 cm^{-1}. The obvious red-shift of the ν(C=O) peak of the dye compared to the raw material is due to the delocalization of the extended π-conjugation in the dye skelton. The peak at 1400 cm^{-1} results from the in-plane bending of C–O–H.

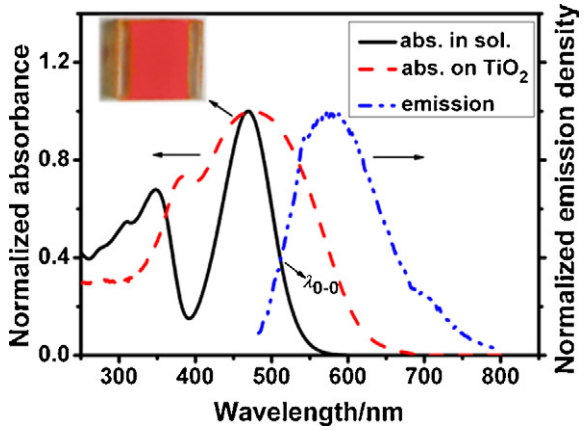

Fig. 5. Normalized absorption (black straight line) and emission spectra (blue dashed line) of TPAR14 in methanol solution as well as the absorption spectrum adsorbed on TiO_2 film (red dashed line). The insert shows the photograph of the TiO_2 electrode coated with TPAR14. (For interpretation of the references to colour in this figure legend, the reader is referred to the web version of the article.)

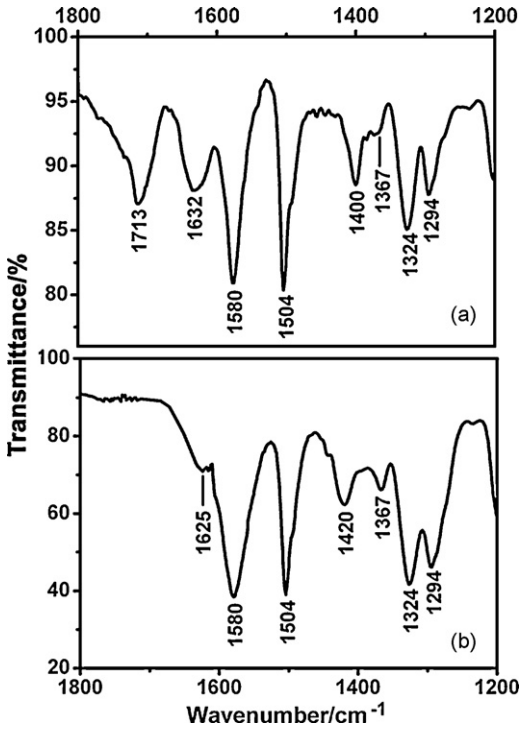

Fig. 6. FT-IR spectra for TPAR14 powder (a) and dye-adsorbed TiO_2 film (b).

After the dye was adsorbed onto the TiO_2 surface, the peaks, diagnostic of –COOH at 1713 and 1400 cm^{-1}, disappeared while a symmetric peak at 1420 cm^{-1} for $-COO^-$ group was observed. The asymmetric absorption for $-COO^-$ group was likely to be mixed with the stretching vibration of C=C in phenyl ring at 1580 cm^{-1} [31], which is observed to be broadened and strengthened. This observation shows that the deprotonation of the –COOH group is taking place on the TiO_2 surface, indicating a bidentate chelating mode for the anchoring of the dye on the TiO_2 surface. The lack of the sharp band of ν(C=O) at 1632 cm^{-1} and the transformation to a broad band at around 1625 cm^{-1} might be the π-conjugated orbital delocalizing over the *J*-aggregate or the direct interaction between the carbonyl group in the rhodanine ring and the TiO_2 surface [32]. Other main vibration bands located at 1504 cm^{-1} for C–C stretching, 1324–1367 cm^{-1} for C–H bending and 1294 cm^{-1} for C=S stretching were not influenced after the dye adsorption onto TiO_2 surface.

3.3. Electrochemical properties

The ground-state oxidation potential $E^0_{D+/D}$ of TPAR14, corresponding to the HOMO level of the dye, was measured to be 0.90 V vs. NHE by DPV. This value is sufficiently more positive than the I_3^-/I^- redox potential (~0.4 V vs. NHE) [33], indicating that the oxidized dye formed after electrons injection into the conduction band of TiO_2 could accept electrons from I^- ions in the electrolyte thermodynamically.

The excited-state oxidation potential $E^0_{D+/D*}$, which reflects the LUMO level of the dye, plays an important role in the electron-injection process. By neglecting any entropy change during light absorption, the value can be derived from the ground-state oxidation couple $E^0_{D+/D}$ and the zero–zero excitation energy E_{0-0} according to the following equation:

$$E^0_{D+/D*} = E^0_{D+/D} - E_{0-0} \quad (3)$$

It is evident that the $E^0_{D+/D*}$ of −1.53 V vs. NHE is more negative than the conduction band edge of TiO_2 (−0.5 V vs. NHE). Therefore,

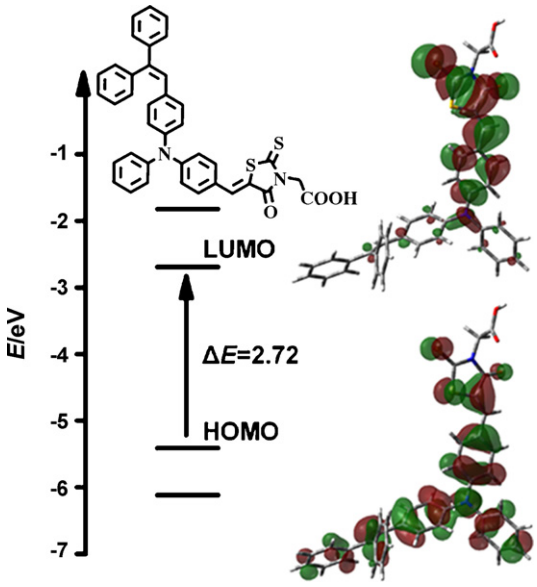

Fig. 7. Schematic representation of the frontier molecular orbitals in vacuo and isodensity surface plots of HOMO and LUMO levels for TPAR14.

this type of sensitizer has sufficient driving force for electron injection to TiO_2 and is very attractive for other semiconductor materials having conduction bands more negative than that of TiO_2. Therefore, TPAR14 can be used as sensitizer for feasible electron transfer in DSCs.

3.4. Calculation analysis

Fig. 7 shows the calculated molecular orbital energy diagram for TPAR14, along with isodensity surface plots of the HOMO and LUMO levels. Observation of the frontier orbitals of the dye in vacuo shows that the HOMO and LUMO are essentially isolated in energy, with the HOMO−1 and LUMO+1 lying ca. 0.7 eV below and above the HOMO and LUMO, respectively. The two phenyl of the diphenylvinyl part are arranged in an out-of-plane fashion to minimize the steric hindrance, which is reflected by the dihedral angle of 57°. The rhodanine-3-acetic acid group was found to be essentially coplanar with the neighboring phenyl of TPA unit, reflecting the strong conjugation across the phenyl ring. The HOMO is to a large extent distributed over the π-system between the donor and acceptor groups, indicating that the binding energy of the electrons in the HOMO is sensitive to a change in the π-system [34]. However, the LUMO reflecting the excited state of the dye under light illumination is a π* orbital delocalized across the 2-(5-benzylidene-4-oxo-2-thioxothiazolidin-3-yl)acetic acid group, with sizable components from the rhodanine-ring part. This distribution of HOMO and LUMO levels is separated in the compound, indicating that the HOMO → LUMO transition can be considered as a charge-transfer transition [35]. Assuming similar molecular orbital geometry when anchored to TiO_2, the position of the LUMO close to the anchoring group enhances the orbital overlap with the titanium 3d orbitals and favors electron injection.

TD-DFT calculations on a B3LYP/6-31+G(d) level of theory show two transitions (Table 1) with large oscillator strengths ($f > 0.1$), consistent with the absorption spectrum. The lowest transition is calculated at 2.18 eV and corresponds to an ICT excitation from HOMO to LUMO. As compared to the experimental absorption maximum at 2.65 eV, the calculated HOMO → LUMO transition is considerably red-shifted, which is related to the extended charge-transfer character [36]. The band experimentally found at 3.56 eV (348 nm) appears to be composed by two almost overlapping

Table 1
Calculated TDDFT excitation energies (eV, nm), oscillator strengths (f), assignment of molecular orbital contributions and character, as compared to experimental absorption band maxima of TPAR14.

#[a]	E (eV, nm)	f	Assignment	Character	Exp. (eV, nm)
1	2.18 (569)	0.83	HOMO → LUMO (0.89)	ICT	2.65 (468)
2	2.90 (426)	0.31	HOMO−1 → LUMO (0.90)	π → π*	3.56 (348)
4	3.17 (392)	0.58	HOMO → LUMO+1 (0.85)	π → π*	3.56 (348)

[a] The ordering number of the calculated excited state.

π → π* transitions (2.90 and 3.17 eV), which are attributed to the combined transitions of HOMO−1 → LUMO and HOMO → LUMO+1. The better agreement between the calculated and experimental absorption energies of the π → π* features as compared to the ICT excitation is related to the localized character of the π → π* excitations, which involve substantially overlapping orbitals.

3.5. DSC performance

Fig. 8a shows the IPCE of the TPAR14-based solar cell. The IPCE spectrum covers the whole visible region in the range of 400–750 nm, facilitating the DSC to efficiently convert solar light to electricity. The IPCE data of TPAR14 sensitizer exhibit a strikingly high efficiency of 85% at 480 nm. When reflection and absorption losses of the FTO glass substrate are considered, the net photon-to-electron conversion efficiency of the dye would almost exceed 90% in its spectral range.

Fig. 8b shows the J–V curve of TPAR14-based solar cell. The detailed photovoltaic parameters are summarized in Table 2, where N3 is included for comparison. As demonstrated in Table 2, TPAR14 gives a high light-to-electricity conversion efficiency of 6.27% with short-circuit photocurrent density (J_{sc}) of 15.5 mA cm^{-2}, open-circuit photovoltage (V_{oc}) of 0.64 V, and FF of 0.63. This conversion efficiency is relatively higher compared to the published results of

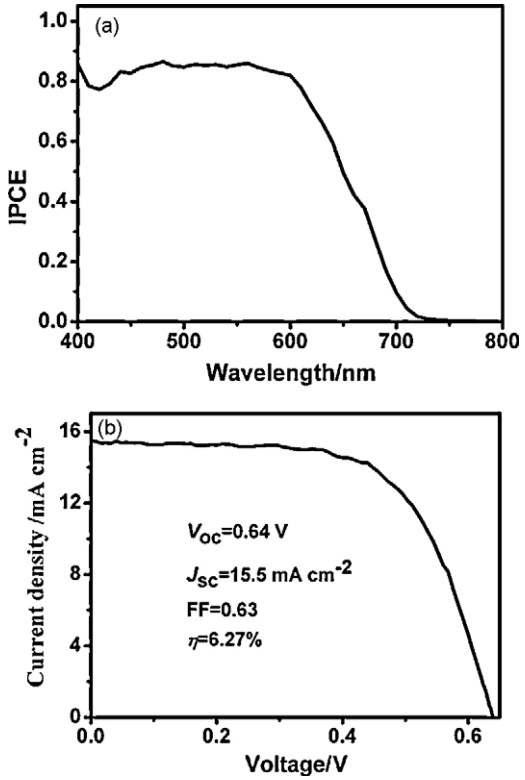

Fig. 8. IPCE (a) and J–V curve (b) of TPAR14-based solar cell (type A).

Table 2
Performance parameters of dye-sensitized solar cells[a].

Dye	V_{oc} (V)	J_{sc} (mA cm^{-2})	FF	η (%)
TPAR14	0.64	15.5	0.63	6.27
N3[b]	0.76	16.4	0.59	7.36

[a] Performance of DSCs (type A) were measured with 0.16 cm^2 working area.
[b] Dye bath: ethanol solution (0.5 mM); electrolyte: 0.6 M DMPImI, 0.1 M LiI, 0.05 M I_2, 0.5 M TBP in dry acetonitrile.

TPA-rhodanine-3-acetic acid-based DSCs [16]. Especially, TPAR14 produced higher J_{sc} and V_{oc} than those of TPAR1 (J_{sc} = 13.9 mA cm^{-2}, V_{oc} = 0.56 V) and TPAR4 (J_{sc} = 15.2 mA cm^{-2}, V_{oc} = 0.58 V) under the same conditions. This improvement is probably due to the stronger electron-donating ability due to the electron transferring from the diphenylvinyl group and the formation of the three-dimensional structure composed by diphenylvinyl group and the adjacent TPA unit. This character could not only depress the interaction between molecules resulting in the energy quenching of the excited states, but also suppress the I_3^- ions in the electrolyte to the TiO_2 surface that is in favor of higher V_{oc}. For comparison, the device with standard N3 dye presents 16.4 mA cm^{-2} of J_{sc}, 0.76 V of V_{oc}, 0.59 of FF, and 7.36% of η under the similar conditions except with additional 0.5 M TBP in the electrolyte. When TBP or another additive such as guanidine thiocyanate (GT) was used for TPAR14 optimizing, the V_{oc} increased, but the J_{sc} decreased largely, resulting in the decrease of η. This result means that either TBP or GT is not suitable for the TPAR14 sensitizer system. The work on searching for more effective additives to increase the efficiency of the DSCs is in progress.

3.6. Stability test

The eventual commercialization of DSCs requires long-term stability of the dye molecule and the cell module. DSCs based on N3 or N719 dyes are reported to have good long-term stability [37]. We therefore investigated the thermal stability of TPAR14 and the stability of cell performance of DSC based on TPAR14. In TG analysis of TPAR14 under N_2 atmosphere, hardly any drop in mass was observed below 300 °C, while the mass dropped sharply higher than 300 °C owing to the decomposition of the dye. It has been reported that decarboxylation of N3 dye occurs at temperatures higher than 290 °C under N_2 [38]. Therefore, TPAR14 has thermal stability that is as good as that of N3 dye.

Fig. 9 shows the stability of a sealed DSC based on TPAR14 stored in dark at 50 °C stress. No sign of dye degradation was observed during the test. The V_{oc} and FF were enhanced moderately from 0.64 to 0.65 V and 0.63 to 0.65, respectively; while the J_{sc} decreased by 8.3% and η was steady-going on the whole. This result suggests

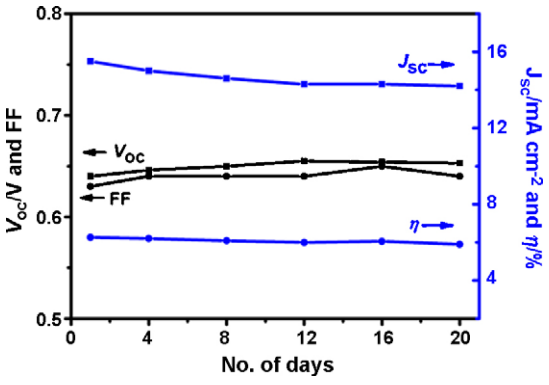

Fig. 9. Short-term evaluation of photovoltaic parameters of sealed DSC based on TPAR14 (type B) under one sun illumination (AM 1.5, 100 mW cm^{-2}).

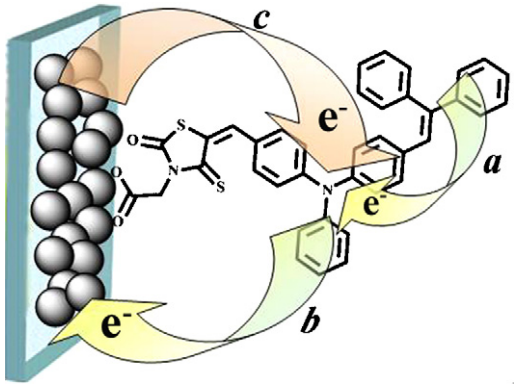

Fig. 10. Schematic representation of electron-transfer processes in dye-sensitized solar cell: (a) electron transfer from the secondary electron donor moiety to the electron donor core; (b) electron injection from electron donor core into the semiconductor; (c) the wasteful charge-recombination pathway of the injected electron with the oxidized dye molecules.

that the dye is relatively stable under heat, where redox electrolyte ions are present.

3.7. Electron transfer process

Based on the above electrochemical properties and photocurrent–voltage characteristics, we describe the relevant electron-transfer process for the TPAR14 sensitized TiO_2 electrode as follows. First, electron transfer from the diphenylvinyl to TPA unit occurs after excitation by visible light, and then the electron is injected into TiO_2. Second, intramolecular electron transfer from TPA to TiO_2 surface causes an interfacial charge separated pair of TiO_2 (e^-)–TPA^+, where the electron is located in the solid TiO_2 and the holes are on TPA (Fig. 10). The diphenylvinyl group takes the function just like an "electron antenna", by which the multi-step charge transfer process results in a relatively longer-lived charge separated state. This process directly leads to an increased photovoltaic performance in the solar cell.

4. Conclusions

In summary, we have successfully synthesized a new TPA derivative TPAR14 with "secondary electron transferring" structure, which is in the combination of an introduction of diphenylvinyl to the adjacent phenyl ring of the TPA core and the rhodanine-3-acetic acid moiety as the acceptor. Density functional theory calculation shows that the electron distribution is shifted from the donor unit to the electron acceptor under light irradiation, which favors efficient ICT. An overall light-to-electricity conversion efficiency of 6.27% is obtained for the DSC with the as-synthesized dye under AM 1.5 irradiation (100 mW cm^{-2}), which is the highest value among the TPA-rhodanine-3-acetic acid-based DSCs. The dye molecule of TPAR14 is relatively stable under heat with a decomposition at 300 °C, while the DSC with TPAR14 shows long-term stability test under heat. The present results strongly suggest that the as-synthesized metal-free organic dye is promising for the application in DSCs.

Acknowledgments

This work was supported by the National Key-Basic Research Program (2005CB623607) and Tianjin High-Tech Development Program (07ZCGHHZ00700).

References

[1] B. O'Regan, M. Grätzel, Nature 353 (1991) 737–740.
[2] L.H. Hu, S.Y. Dai, J. Weng, S.F. Xiao, Y.F. Sui, Y. Huang, S.H. Chen, F.T. Kong, X. Pan, L.Y. Liang, K.J. Wang, J. Phys. Chem. B 111 (2007) 358–362.
[3] Z.G. Chen, Y.W. Tang, H. Yang, Y.Y. Xia, F.Y. Li, T. Yi, C.H. Huang, J. Power Sources 171 (2007) 990–998.
[4] M.K. Nazeeruddin, F.D. Angelis, S. Fantacci, A. Selloni, G. Viscardi, P. Liska, S. Ito, B. Takeru, M. Grätzel, J. Am. Chem. Soc. 127 (2005) 16835–16847.
[5] Q.H. Yao, L. Shan, F.Y. Li, D.D. Yin, C.H. Huang, New J. Chem. 27 (2003) 1277–1283.
[6] K. Hara, T. Sato, R. Katoh, A. Furube, Y. Ohga, A. Shinpo, S. Suga, K. Sayama, H. Sugihara, H. Arakawa, J. Phys. Chem. B 107 (2003) 597–606.
[7] Z.S. Wang, N. Koumura, Y. Cui, M. Takahashi, H. Sekiguchi, A. Mori, T. Kubo, A. Furube, K. Hara, Chem. Mater. 20 (2008) 3993–4003.
[8] K. Hara, Y. Tachibana, Y. Ohga, A. Shinpo, S. Suga, K. Sayama, H. Sugihara, H. Arakawa, Sol. Energy Mater. Sol. Cells 77 (2003) 89–103.
[9] H.N. Tian, X.C. Yang, R.K. Chen, R. Zhang, A. Hagfeldt, L.C. Sun, J. Phys. Chem. C 112 (2008) 11023–11033.
[10] W.H. Zhan, W.J. Wu, J.L. Hua, Y.H. Jing, F.S. Meng, H. Tian, Tetrahedron Lett. 48 (2007) 2461–2465.
[11] H. Qin, S. Wenger, M.F. Xu, F.F. Gao, X.Y. Jing, P. Wang, S.M. Zakeeruddin, M. Grätzel, J. Am. Chem. Soc. 130 (2008) 9202–9203.
[12] Z.G. Chen, F.Y. Li, C.H. Huang, Curr. Org. Chem. 11 (2007) 1241–1258.
[13] D. Liu, R.W. Fessenden, G.L. Hug, P.V. Kamat, J. Phys. Chem. B 101 (1997) 2583–2590.
[14] P. Wei, X.D. Bi, Z. Wu, Z. Xu, Org. Lett. 7 (2005) 3199–3202.
[15] W. Xu, J. Pei, J.F. Shi, S.J. Peng, J. Chen, J. Power Sources 183 (2008) 792–798.
[16] M. Liang, W. Xu, F.S. Cai, P. Chen, B. Peng, J. Chen, Z. Li, J. Phys. Chem. C 111 (2007) 4465–4472.
[17] T. Kitamura, M. Ikeda, K. Shigaki, Chem. Mater. 16 (2004) 1806–1812.
[18] S. Ito, S.M. Zakeeruddin, R. Humphry-Baker, P. Liska, R. Charvet, P. Comte, M.K. Nazeeruddin, P. Péchy, M. Takata, H. Miura, S. Uchida, M. Grätzel, Adv. Mater. 18 (2006) 1202–1205.
[19] S. Hattori, K. Ohkubo, Y. Urano, H. Sunahara, T. Nagano, Y. Wada, N.V. Tkachenko, H. Lemmetyinen, S. Fukuzumi, J. Phys. Chem. B 109 (2005) 15368–15375.
[20] X.H. Li, J. Gui, H. Yang, W.J. Wu, F.Y. Li, H. Tian, C.H. Huang, Inorg. Chim. Acta 361 (2008) 2835–2840.
[21] S.Y. Jang, V. Seshadri, M.S. Khil, A. Kumar, M. Marquez, P.T. Mather, G.A. Sotzing, Adv. Mater. 17 (2005) 2177–2180.
[22] P. Bonhôte, A.P. Dias, N. Papageorgiou, K. Kalyanasundaram, M. Grätzel, Inorg. Chem. 35 (1996) 1168–1178.
[23] K. Ebitani, K. Motokura, K. Mori, T. Mizugaki, K. Kaneda, J. Org. Chem. 71 (2006) 5440–5447.
[24] R. Greenwald, M. Chaykovsky, E.J. Corey, J. Org. Chem. 28 (1963) 1128–1129.
[25] G. Lai, X.R. Bu, J. Santos, E.A. Mintz, Synlett (1997) 1275–1276.
[26] R.R. Gagńe, C.A. Koval, G.C. Lisensky, Inorg. Chem. 19 (1980) 2854–2855.
[27] M.J. Frisch, G.W. Trucks, H.B. Schlegel, G.E. Scuseria, M.A. Robb, J.R. Cheeseman Jr., J.A. Montgomery, T. Vreven, K.N. Kudin, J.C. Burant, J.M. Millam, S.S. Iyengar, J. Tomasi, V. Barone, B. Mennucci, M. Cossi, G. Scalmani, N. Rega, G.A. Petersson, H. Nakatsuji, M. Hada, M. Ehara, K. Toyota, R. Fukuda, J. Hasegawa, M. Ishida, T. Nakajima, Y. Honda, O. Kitao, H. Nakai, M. Klene, X. Li, J.E. Knox, H.P. Hratchian, J.B. Cross, C. Adamo, J. Jaramillo, R. Gomperts, R.E. Stratmann, O. Yazyev, A.J. Austin, R. Cammi, C. Pomelli, J.W. Ochterski, P.Y. Ayala, K. Morokuma, G.A. Voth, P. Salvador, J.J. Dannenberg, V.G. Zakrzewski, S. Dapprich, A.D. Daniels, M.C. Strain, O. Farkas, D.K. Malick, A.D. Rabuck, K. Raghavachari, J.B. Foresman, J.V. Ortiz, Q. Cui, A.G. Baboul, S. Clifford, J. Cioslowski, B.B. Stefanov, G. Liu, A. Liashenko, P. Piskorz, I. Komaromi, R.L. Martin, D.J. Fox, T. Keith, M.A. Al-Laham, C.Y. Peng, A. Nanayakkara, M. Challacombe, P.M.W. Gill, B. Johnson, W. Chen, M.W. Wong, C. Gonzalez, J.A. Pople, Gaussian 03, Revision C. 01, Gaussian, Inc., Wallingford, CT, 2004.
[28] F.J. Li, F.Y. Cheng, J.F. Shi, F.S. Cai, M. Liang, J. Chen, J. Power Sources 165 (2007) 911–915.
[29] S. Roquet, A. Cravino, P. Leriche, O. Alévêque, P. Frère, J. Roncali, J. Am. Chem. Soc. 128 (2006) 3459–3466.
[30] M.K. Nazeeruddin, A. Kay, I. Rodicio, R. Humphry-B, E. Müller, P. Liska, N. Vlachopoulos, M. Grätzel, J. Am. Chem. Soc. 115 (1993) 6382–6390.
[31] J.K. Feng, Y.L. Cao, X.P. Ai, H.X. Yang, J. Power Sources 177 (2008) 199–204.
[32] K. Sayama, S. Tsukagoshi, K. Hra, Y. Ohga, A. Shinpou, Y. Abe, S. Suga, H. Arakawa, J. Phys. Chem. B 106 (2002) 1363–1371.
[33] A. Hagfeldt, M. Grätzel, Chem. Rev. 95 (1995) 49–68.
[34] P. Qin, X. Yang, R. Chen, L. Sun, T. Marinado, T. Edvinsson, G. Boschloo, A. Hagfeldt, J. Phys. Chem. C 111 (2007) 1853–1861.
[35] V. Lemaur, M. Steel, D. Beljonne, J.L. Brédas, J. Cornil, J. Am. Chem. Soc. 127 (2005) 6077–6086.
[36] S. Kim, J.K. Lee, S.O. Kang, J. Ko, J.H. Yum, S. Fantacci, F.D. Angelis, D.D. Censo, M.K. Nazeeruddin, M. Grätzel, J. Am. Chem. Soc. 128 (2006) 16701–16707.
[37] P.M. Sommeling, M. Späth, H.J.P. Smit, N.J. Bakker, J.M. Kroon, J. Photochem. Photobiol. A 164 (2004) 137–144.
[38] M. Amirnasr, M.K. Nazeeruddin, M. Grätzel, Thermochim. Acta 348 (2000) 105–114.